

Classical analogs for Rabi-oscillations, Ramsey-fringes, and spin-echo in Josephson junctions

Jeffrey E. Marchese

Department of Applied Science, University of California, Davis, California 95616, USA

Matteo Cirillo

Dipartimento di Fisica and INFM, Università di Roma "Tor Vergata", I-00173 Roma, Italy

Niels Grønbech-Jensen

Department of Applied Science, University of California, Davis, California 95616, USA

(To appear in "Nonlinear Waves in Complex Systems: Energy Flow and Geometry", eds. M.P.Sørensen and J.G.Caputo)

Abstract. We investigate the results of recently published experiments on the quantum behavior of Josephson circuits in terms of the classical modelling based on the resistively and capacitively-shunted (RCSJ) junction model. Our analysis shows evidence for a close analogy between the nonlinear behavior of a pulsed microwave-driven Josephson junction at low temperature and low dissipation and the experimental observations reported for the Josephson circuits. Specifically, we demonstrate that Rabi-oscillations, Ramsey-fringes, and spin-echo observations are not phenomena with a unique quantum interpretation. In fact, they are natural consequences of transients to phase-locking in classical nonlinear dynamics and can be observed in a purely classical model of a Josephson junction when the experimental recipe for the application of microwaves is followed and the experimental detection scheme followed. We therefore conclude that classical nonlinear dynamics can contribute to the understanding of relevant experimental observations of Josephson response to various microwave perturbations at very low temperature and low dissipation.

1. Introduction

In recent years the possibility of employing Josephson junctions circuitry as solid state elements for quantum information processing has been investigated by several groups and authors both at theoretical and experimental levels [1]. At temperatures low enough, operating the electronic Josephson devices in the regime where the thermal energy is smaller than the energy spacing between quantum mechanical energy levels, interpretation of experimental results in terms of quantum response has been reported in a number of publications [2, 3, 4, 5, 6, 7, 8, 9, 10, 11, 12]. Specific key observations that are being used to characterize the nature of a Josephson system at these extremely low temperatures are usually linked to the system response to a variety of pulsed microwave applications. The reason is at

least tri-fold. First, due to the nature of the Josephson effect, it is not easy to make direct observations of the expected quantum states in the anharmonic potential of a zero-mean voltage state Josephson system, which is the state of interest, so convenient probes of the system are those where transitions from zero-voltage states to non-zero states can be induced with different probability depending on the nature of the initial zero-voltage state of the system. Second, the analogy between a single degree of freedom quantum Josephson system and a more traditional quantum system allows for useful characterization tools for Josephson applications of quantum mechanical features from, e.g., atomic systems, to infer the quantum behavior of the system from concepts such as Rabi oscillations [14], Ramsey fringes [15], and spin echo. Third, the control and manipulation of the state of the system is conveniently directed through microwave frequencies that are commensurate with the anticipated energy level spacings in the zero-voltage Josephson state. The understanding of the Josephson response to pulsed microwave applications is therefore critical for the interpretation of experimental observables.

A classical nonlinear oscillator, which is subjected to pulsed time-varying perturbations, may exhibit several phenomena that are relevant for microwave perturbed Josephson systems. For example, an anharmonic oscillator provides an amplitude-dependent resonance frequency, which, in turn, relates resonance frequency directly to system energy [13, 16]. Also, the transient system behavior, due to an onset of resonant microwave application to a low-dissipation Josephson system, can give rise to low frequency amplitude and phase modulations in the system response [16, 17, 18, 19]. It has been shown that these phenomena in classical nonlinear dynamics are not unlike what one would expect from a comparable quantum system responding to a microwave signal, which is resonant with the intrinsic energy level spacing of the potential energy surface. In fact, the simplest possible classical Josephson system, a single Josephson junction, has been shown to exhibit phenomena of resonant escape from the anharmonic potential well [20, 21, 22], as well as transient slow modulations to phase-locking closely resembling experimental observations of Rabi-oscillations and Ramsey-fringes in Josephson circuits [16, 19, 23]. The correspondence is further substantiated by conducting numerical simulations of the classical Josephson model in accordance with the experimental procedures, and extracting the resulting data as it is done experimentally; namely as a statistical probability of escape from the Josephson potential well. Also, it has been observed that the classical model exhibits the phenomena of interest in the limits of low temperature and low dissipation (high-Q), consistent with reported experiments. With the demonstration of close classical analogies to Rabi-oscillations and Ramsey-fringes, which are themselves closely related phenomena, we here extend the investigation of the classical model to also include a demonstration of the classical equivalent to the spin-echo observations [2, 4], since these represent yet another manifestation of the transient modula-

tions (Rabi-oscillations) in the approach to a phase-locked (excited) dynamical state. The work described here is primarily meant to demonstrate the phenomena in question in the most simple system possible; the single Josephson junction. However, while we will here limit ourselves to a descriptive treatment of a simple system, the phenomena are obvious and ubiquitous to a broad range of classical Josephson circuits, including one or more superconducting loops containing one or more Josephson junctions manipulated through magnetic fields imposed on the loops.

2. The Model

The normalized classical equation for a perturbed Josephson junction within

$$\ddot{\varphi} + \alpha\dot{\varphi} + \sin\varphi = \eta + \varepsilon_s(t)\sin(\omega_s t + \theta_s) + \varepsilon_p(t) + n(t),$$

where φ is the difference between the phases of the quantum mechanical wave functions defining the junction, η represents the dc bias current, and $\varepsilon_s(t)$, ω_s , and θ_s represent microwave amplitude, frequency, and phase, respectively. All currents are normalized to the critical Josephson current I_c , and time is measured in units of the inverse Josephson plasma frequency, ω_0^{-1} , where $\omega_0^2 = 2eI_c/\hbar C = 2\pi I_c/\Phi_0 C$, C being the capacitance of the junction, and $\Phi_0 = h/2e = 2.07 \times 10^{-15} \text{ Wb}$ is the flux quantum. Tunneling of quasiparticles is represented by the dissipative term, where $\alpha = \hbar\omega_0/2eRI_c$ is given by the shunt resistance R , and the accompanying thermal fluctuations are defined by the dissipation-fluctuation relationship [25]

$$\langle n(t) \rangle = 0 \quad (1)$$

$$\langle n(t_1)n(t_2) \rangle = 2\alpha \frac{k_B T}{H_J} \delta(t_2 - t_1) = 2\alpha \Theta \delta(t_2 - t_1), \quad (2)$$

T being the thermodynamic temperature, H_J is the characteristic Josephson energy $H_J = I_c \hbar/2e$, and $\Theta = k_B T/H_J$ is thereby defined as the normalized temperature (or normalized thermal energy). In order to give orders of magnitudes for the typical realistic parameters we indicate that a good quality Josephson junction having a critical current of $I_c = 5 \mu\text{A}$ and fabricated in the standard Nb-trilayer technology [26] may have R (usually identified with the subgap resistance) in the range $(3 - 6)k\Omega$, a capacitance $C \cong 5\text{pF}$, $\nu_0 = \omega_0/2\pi \cong 9\text{GHz}$, α in the range $(10^{-3} - 10^{-4})$, $H_J \cong 16 \times 10^{-22} \text{ J}$. The values of R and α in the specified interval depend on the quality of the junctions.

A current pulse for probing the state of the system is represented by $\varepsilon_p(t)$. Figure 2 sketches the signaling details relevant for the observations of Rabi-oscillations (Fig. 2a), Ramsey-fringes (Fig. 2b), and spin-echo (Fig. 2c). The system is initially in its zero-voltage state (thermalized in the potential well illustrated in Figure 1b), when a microwave is applied in a single interval or in a sequence of pulses, which

have the same reference phase θ_s . Due to the subsequent application of the probe pulse $\varepsilon_p(t)$, the system variable φ may escape the potential well, and the amplitudes of $\varepsilon_p(t)$ is parameterized such that probe pulse induced escape is likely if the system energy, relative to the potential well depth, is significant at the time immediately prior to the onset of $\varepsilon_p(t)$, and unlikely otherwise. By conducting a large number of such simulations, each with identical parameters, except for θ_s , which is chosen from a uniform distribution in the interval $]0, 2\pi]$, and the thermal noise current, a statistical signature of the system energy due to the signaling strategy given by $\varepsilon_s(t)$ can be inferred from the resulting switching probability. This information can be directly obtained in simulations by calculating the defined normalized energy

$$H = \frac{1}{2}\dot{\varphi}^2 + 1 - \cos \varphi - \eta\varphi ,$$

where the minimum of the potential well can be represented by the energy

$$H_0 = 1 - \sqrt{1 - \eta^2} - \eta \sin^{-1} \eta .$$

The above statistical procedure of monitoring the probability of escape is applied experimentally, since direct measurements of the energy content in a zero-average voltage state is not possible. We therefore mimic the experimental procedure in our simulations in order to make direct linkage between modeling and experimental observations of switching probabilities. We finally notice two essential system parameters that are related to the choice of bias point η ; namely microwave frequency ω_s and temperature Θ . The microwave frequency should be chosen such that resonant states can be excited in the vicinity of $\omega_s^2 \approx \omega_l^2 = \sqrt{1 - \eta^2}$, and the thermal energy Θ should be significantly smaller than the potential well depth $\Theta \ll \Delta U = 2\sqrt{1 - \eta^2} + 2\eta \sin^{-1} \eta - \pi\eta$, ensuring that recorded switching events are not simply a reflection of thermal activation.

3. Simulation Details and Results

Following the procedure of reported experiments, we record the switching from the zero-voltage state ($\langle \dot{\varphi} \rangle = 0$) as a result of applying the three different recipes sketched in Figure 2. We will, unless otherwise noted, throughout this presentation use the following parameters: $\eta = 0.904706$, which is equivalent to a linear resonance frequency $\omega_l = \sqrt[4]{1 - \eta^2} = 0.652714$, $\alpha = 10^{-4}$, which provides a high-Q resonator, and, when temperature is applied, $\Theta = 2 \times 10^{-4} \ll \Delta U = 5.57 \times 10^{-2}$.

3.1. RABI-OSCILLATIONS

The first signaling procedure is shown in Figure 2a, where the Josephson junction (Equation (1)) is initially resting in the potential well, when the microwave pulse is initiated. We use a microwave frequency $\omega_s = \omega_l$, but we note that this

is not a requirement for the observations of this work [16]. Figure 3 shows the evolution for $\Theta = 0$ of the junction phase $\varphi(t)$ and the system energy $H(t) - H_0$ for a microwave pulse with amplitude $\epsilon_s = 0.00217$. Several important features can be extracted from this figure. First, we observe how the junction is driven into a phase-locked state by the microwave application. Second, we observe how the junction response is modulated by a low frequency envelope function that causes the system energy to oscillate around the steady-state phase-locked energy. Third, comparing two different durations of microwave pulses, we illustrate how the microwave duration influences the switching probability when the probe pulse is applied after the termination of the microwave field. Figures 3a and 3b show how the probe pulse catches the system in a low energy state, resulting in a "no-switch" count, and Figures 3c and 3d show the probe pulse catching the system in a high energy state, resulting in a "switch" count. Thus, by varying the duration of the microwave pulse, we can observe the slow modulation frequency of the transient to the phase-locked state in the zero-voltage state of the junction by observing the switching statistics by the probe pulse application. Such statistics is shown in Figure 4a for $\Theta = 2 \times 10^{-4}$, where the switching probability as a function of microwave duration is displayed for averages of 2500 possible switching events. Clearly, the probability exhibits the slow modulation seen in Figure 3, and these are the classical analogues to Rabi-oscillations [16, 19]. These oscillations have a reasonably well-defined frequency. The amplitude decays for several reasons, including the dissipation α , which sets a time scale for the transients to phase-locking [16], thermal effects, which provides decoherence to the evolution, and the random phase θ_s , which dephases the different trajectories that are averaged to give Figure 4a. Based on Figure 4a, we can now extend the analogy to quantum mechanics by noticing that a microwave pulse of one Rabi-period $\tau_R = 2\pi/\Omega_R$, where Ω_R is the modulation (Rabi) frequency, leaves the system energy in roughly the same state as before the microwave pulse was applied. We therefore denote such a pulse a 2π -pulse. Similarly, we define a π -pulse to be one of duration $\tau_R/2$, and a $\pi/2$ -pulse represents a duration $\tau_R/4$, which is the duration it takes from the microwave onset to elevate the system to its steady state energy.

3.2. RAMSEY-FRINGS

Following the recipe outlined in, e.g., Ref. [2, 4] we can now apply a sequence of controlled microwave pulses, such as illustrated in Figure 2b, where two $\pi/2$ pulses are applied with a delay before the probe pulse determines if the resulting state has enough energy to be perturbed into escape. Figure 5 illustrates, in analogy with Figure 3 for $\Theta = 0$, the two characteristic outcomes of temporal evolutions of the system dynamics for two different time intervals between the $\pi/2$ -pulses. The first pulse elevates the system energy to the intermediate level, where it is left to evolve freely after the first pulse is terminated. During the time between

the two pulses, the microwave field and the junction oscillate at almost the same frequency, but with a small detuning of the mutual phase. Thus, this ballistic interval can produce very different outcomes when the second $\pi/2$ -pulse is applied, depending on the time interval. If the time interval is such that the second pulse is initiated with a mutual phase difference to the junction similar to when the first pulse terminated, then the second pulse will continue to pump energy into the junction, elevating its energy to the maximum at the conclusion of the second pulse. This scenario is shown in Figures 5c and 5d, where the probe pulse triggers an escape event. However, if the second $\pi/2$ -pulse is initiated such that the relative phase is opposite to what it was when the first pulse was terminated, then the second pulse will attenuate the energy of the junction, leaving it with very low energy at the conclusion of the second pulse. This scenario is illustrated in Figures 5a and 5b, where the probe pulse cannot induce an escape event. The switching probability as a function of the ballistic time interval between the two $\pi/2$ -pulses is shown for $\Theta = 2 \times 10^{-4}$ and microwave frequency $\omega_s = \omega_l$ in Figure 4b. The clearly visible oscillations in the switching probability are the classical equivalent of quantum mechanical Ramsey-fringes. As was the case for the Rabi-oscillations, the visible Ramsey-fringes have a reasonably well defined frequency Ω_F and an attenuating amplitude, where the attenuation is due to a combination of dissipation, thermalization, and the averaging over trajectories of different random microwave phases θ_s . The close relationship between the classical observation shown here and quantum mechanical Ramsey-fringes can be further underlined by evaluating the Ramsey-fringe frequency Ω_F as a function of frequency detuning from the harmonic resonance frequency ω_l . This is shown in Figure 6, where black markers and associated error bars represent the measured Ramsey-fringe frequency. We clearly observe the characteristic unity-slope ("V"-shape indicated by the dashed lines) dependency on the frequency detuning from linear resonance [10]. An obvious deviation from a naive expectation is that the microwave frequency for which $\Omega_F = 0$ is not exactly the linear resonance. This is due to the anharmonicity of the potential as well as to the dissipation in the system. The Ramsey-fringe frequency Ω_F is drifting slightly toward higher values as the $\pi/2$ -pulse separation is increased. This is because higher oscillation amplitudes result in lower resonance frequencies. Thus, defining the Ramsey-fringe frequency from the first couple of oscillations (the ones with the best resolution) will make Ω_F susceptible to the anharmonicity of the potential. This, in turn, will make the ballistic evolution between the two $\pi/2$ -pulses commensurate with a slightly detuned microwave frequency such that $\Omega_F = 0$ for $\omega_s < \omega_l$; which is what can be observed in Figure 6a. Figure 6b illustrates how increasing the dissipation parameter to $\alpha = 10^{-3}$ will provide a faster linearization of the resonance frequency of the junction, resulting in the expected shift in the characteristic point where $\Omega_F = 0$ for $\omega_s \approx \omega_l$.

3.3. SPIN-ECHO

We finally study the result of applying the signaling protocol shown in Figure 2c. This protocol is similar to the one resulting in Ramsey-fringes, but a π -pulse is inserted between the two $\pi/2$ -pulses in order to mimic a 180° phase shift in the modulation dynamics. In analogy with experimental observations of spin-echo in Josephson systems [2, 4] we choose a temporal separation between the two $\pi/2$ -pulses, and observe the switching characteristics of the junction, when the probe pulse is applied, as a function of the temporal position of the π -pulse, which serves as a 180° phase-shift from which an "echo" can be detected. Since the system either switches or remains in the potential well after the application of the probe, we can again demonstrate the typical dynamics by the two cases shown for $\Theta = 0$ in Figure 7. Here we have chosen a total normalized time interval for the $\pi/2$ -pulses of 2500 time units. The first case, which is displayed in Figures 7a and 7b, shows that the application of the π -pulse only has a marginal effect on the evolution of the phase and its energy. Since the second $\pi/2$ -pulse is initiated out of phase with the junction, the subsequent probe pulse perturbation cannot make the system escape the potential well. In contrast, Figures 7c and 7d show that a slightly different timing in the application of the π -pulse will provide a resonant increase in the system oscillation amplitude and energy. Further, the phase-relationship between the microwave field and the junction is now such that the second $\pi/2$ -pulse enhances the energy of the system. This results in an escape event when the probe pulse is applied. The probability of switching as a function of the timing of π -pulse initiation is shown in Figure 4c for $\Theta = 2 \times 10^{-4}$ and $\omega_s = 0.965\omega_l$. We find very clear signatures of the oscillations in the switching probability, which can be interpreted as the phase-dependency of the "echo" that either leaves the system in high or low energy states. Thus, this is the classical Josephson analogue to quantum mechanical spin-echo. We again notice that the oscillations provide a certain frequency, which we have displayed in Figure 6a as open markers as a function of microwave frequency detuning. It is obvious that the frequency is closely related to the Ramsey-fringe frequency Ω_F , except near the point $\Omega_F = 0$. This deviation can be directly associated with the drift in frequency due to anharmonicity that we mentioned above for the Ramsey-fringes, and the exact values of the spin-echo oscillations seem to depend strongly on which part of the curve (such as the one shown in Figure 4c) is used to calculate the frequency when the oscillation frequency is small.

4. Conclusions

Just like spectroscopic resonant multi-peak switching distributions can be observed and explained within a classical Josephson framework [20], so can the phenomena of Rabi-oscillations, Ramsey-fringes, and spin-echo be observed in the

purely classical Josephson model by following the recipe of the experimental observations. We have here tried to outline this observation in the simplest possible system; namely the single Josephson junction. This is not a direct representation of specific experimental configurations, which are much more complex, although the parameter values chosen here have been inspired by several relevant experiments. Considering the simplicity of the single junction and the modeling approach in this presentation, the overall agreement between the classical results and experimental observations is remarkable. Not only do we observe the abovementioned phenomena in the simple classical model, but we also observe the magnitudes of, and relationships between, the various oscillations in the respective switching distributions to be quite reasonably aligned with experimental observations and expectations. We therefore submit that much in the interpretation of the experiments on microwave manipulations of Josephson systems at low temperature and low dissipation can be contributed from the well known and well documented classical Josephson dynamics.

5. Acknowledgment

This work was supported in part by the UC Davis Center for Digital Security, AFOSR grant FA9550-04-1-0171, in part by MIUR (Italy) COFIN04.

Bibliography

1. *Quantum Computing and Quantum Bits in Mesoscopic Systems*, A. Leggett, B. Ruggiero, and P. Silvestrini, Eds. (Kluwer Academic/Plenum Publishers, New York, 2004).
2. D. Vion, A. Aasime, A. Cottet, P. Joyez, H. Pothier, C. Urbina, D. Esteve, and M. H. Devoret, *Science* **296**, 886 (2002).
3. J. M. Martinis, S. Nam, J. Aumentado, *Phys. Rev. Lett.* **89**, 117901 (2002).
4. D. Vion, A. Aasime, A. Cottet, P. Joyez, H. Pothier, C. Urbina, D. Esteve, and M. H. Devoret, *Fortschr. Phys.* **51**, 462 (2003).
5. J. M. Martinis, S. Nam, J. Aumentado, K. M. Lang, *Phys. Rev. B* **67**, 094510 (2003).
6. I. Chiorescu, Y. Nakamura, C. J. P. M. Harmans, J. E. Mooij, *Science* **299**, 1869 (2003).
7. J. Claudon, F. Balestro, F. W. J. Hekking, O. Buisson, *Phys. Rev. Lett.* **93**, 187003 (2004).
8. T. Kutsuzawa, H. Tanaka, S. Saito, H. Nakano, K. Semba, H. Takayanagi, *Appl. Phys. Lett.* **87**, 073501 (2005).
9. A. Wallraff, D. I. Schuster, A. Blais, L. Frunzio, J. Majer, M. Devoret, S. M. Girvin, R. J. Schoelkopf, *Phys. Rev. Lett.* **95**, 060501 (2005).
10. B. L. T. Plourde, T. L. Robertson, P. A. Reichart, T. Hime, S. Linzen, C. Wu, J. Clarke, *Phys. Rev. B* **72**, 060506 (2005).
11. R. H. Koch, J. R. Rozen, G. A. Keefe, F. M. Milliken, C. C. Tsuei, J. R. Kirtley, D. P. DiVincenzo, *Phys. Rev. B* **72**, 092512 (2005).
12. R. W. Simmonds, K. M. Lang, D. A. Hite, S. Nam, D. P. Pappas, and J. M. Martinis, *Phys. Rev. Lett.* **93**, 077003 (2004).

13. N. F. Pedersen, M. R. Samuelsen, and K. Sørmark, J. Appl. Phys. **44**, 5120 (1973).
14. I. I. Rabi, Phys. Rev. Lett. **51**, 652 (1937).
15. N. F. Ramsey, Phys. Rev. **78**, 695 (1950).
16. J. E. Marchese, M. Cirillo, N. Grønbech-Jensen, Phys. Rev. B **73**, 174507 (2006).
17. P. S. Lomdahl and M. R. Samuelsen, Phys. Lett. A **128**, 427 (1988).
18. N. Grønbech-Jensen, Y. S. Kivshar, and M. R. Samuelsen, Phys. Rev. B **47**, 5013 (1993).
19. N. Grønbech-Jensen and M. Cirillo, Phys. Rev. Lett. **95**, 067001 (2005).
20. N. Grønbech-Jensen, M. G. Castellano, F. Chiarello, M. Cirillo, C. Cosmelli, L. V. Filippenko, R. Russo, and G. Torrioli, Phys. Rev. Lett. **93**, 107002 (2004).
21. N. Grønbech-Jensen, M. G. Castellano, F. Chiarello, M. Cirillo, C. Cosmelli, V. Merlo, R. Russo, and G. Torrioli, in *Quantum Computing: Solid State Systems*, p. 111, edited by B. Ruggiero, P. Delsing, C. Granata, Y. Paskin, and P. Silvestrini (Kluwer Academic/Springer Publishers, New York, 2006).
22. M. Cirillo, P. Carelli, M. G. Castellano, F. Chiarello, C. Cosmelli, N. Grønbech-Jensen, R. Leoni, J. E. Marchese, F. Mattioli, D. Simeone, and G. Torrioli, Physica C **437-438**, 46 (2006).
23. J. E. Marchese, M. Cirillo, and N. Grønbech-Jensen, Open Sys. & Information Dyn. **14**, 1 (2007).
24. A. Barone and G. Paternò, *Physics and Applications of the Josephson Effect* (Wiley, New York 1982).
25. G. Parisi, *Statistical Field Theory* (Addison-Wesley, Redding, MA, 1988).
26. S. Morohashi and S. Hasuo, J. Appl. Phys. **61**, 4835 (1987).

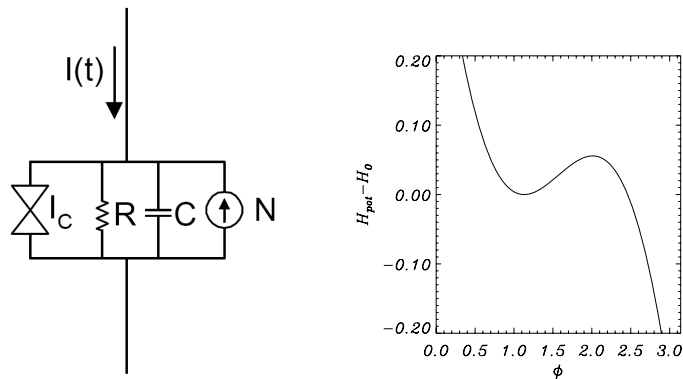


Fig. 1: Sketch of the RCSJ model where $I/I_c = \eta + \varepsilon_s(t) \sin(\omega_s t + \theta) + \varepsilon_p(t)$ and $N = n(t)I_c$. Also shown is the Josephson potential for $\eta = 0.904706$.

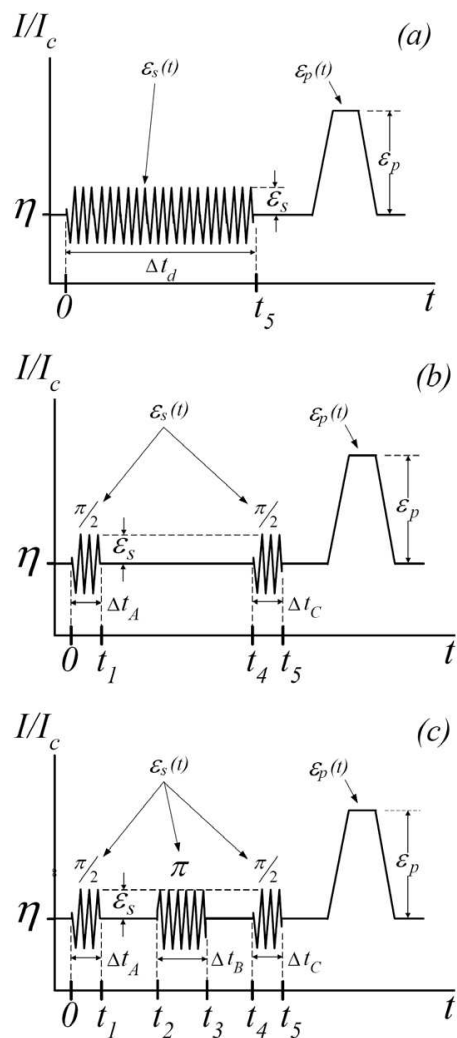


Fig. 2: Signalling diagrams for simulating (a) Rabi-type oscillations (b) Ramsey-type fringes and (c) spin-echo-type oscillations.

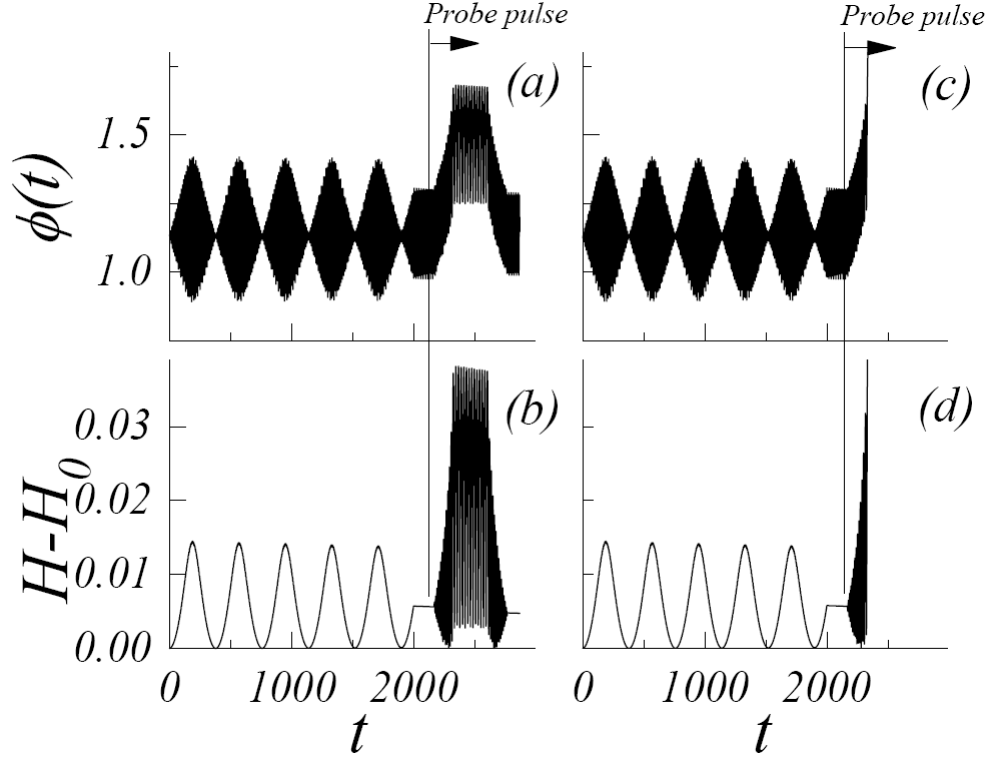


Fig. 3: Direct simulation of the Rabi-type oscillation switching response. Josephson junction response to the sequential application of two $\pi/2$ microwave pulses followed by a probe field. Panels (a,b) show phase-difference and energy for a non-switching sequence. Panels (c,d) indicate a switching event. Switching and non-switching events trigger according to a randomly determined phase. Parameters were $\alpha = 10^{-4}$, $\eta = 0.904706$, $\varepsilon_s = 2.17 \times 10^{-3}$, $\omega_s = \omega_l = \sqrt[4]{1 - \eta^2} = 0.652714$, $\varepsilon_p = 8.2 \times 10^{-2}$, and $\Theta = 0$.

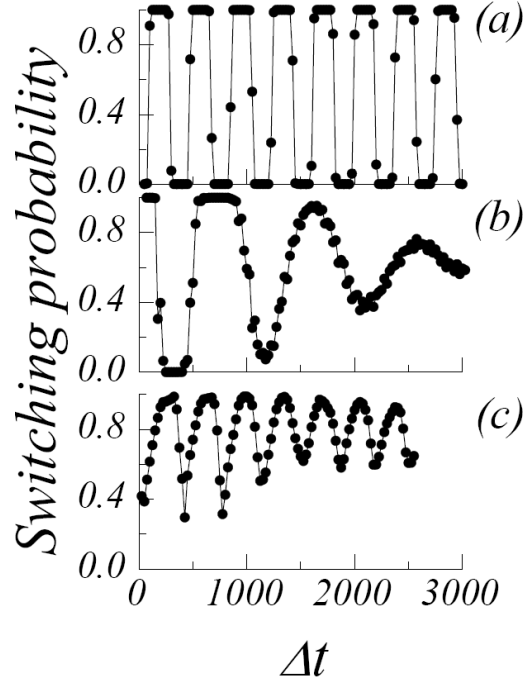


Fig. 4: Switching probabilities for (a) Rabi-type oscillations, (b) Ramsey-type fringe and (c) Spin-echo-type simulations. Each point represents statistics of $\sim 2,500$ events at $\Theta = 2.00 \times 10^{-4}$. The horizontal axis in panel (a) represents the duration Δt_d of the microwave pulse. In panel (b) the horizontal axis indicates the $\pi/2$ -pulse separation $(t_4 - t_1)$. Panel (c) has the period between the end of the first $\pi/2$ -pulse and the beginning of the π -pulse – i.e., the π -pulse offset $(t_2 - t_1)$. In panels (a) & (b) the driving frequency is the linear resonance frequency $\omega_s = \omega_l = \sqrt[4]{1 - \eta^2} = 0.652714$. In (c) the driving frequency is $\omega_s = 0.965\omega_l$. The magnitude of the probe pulse in (a) & (b) $\varepsilon_p = 8.2 \times 10^{-2}$. The probe pulse in panel (c) is $\varepsilon_p = 7.5 \times 10^{-2}$. Panel (c) reflects data from spin-echo-type simulations for $t_4 - t_1 = 2750$. Common to all panels are the characteristic damping $\alpha = 10^{-4}$ and the microwave signal amplitude $varepsilon_{\text{psilon}}_s = 2.17 \times 10^{-3}$. Lines are added to aid the eye.

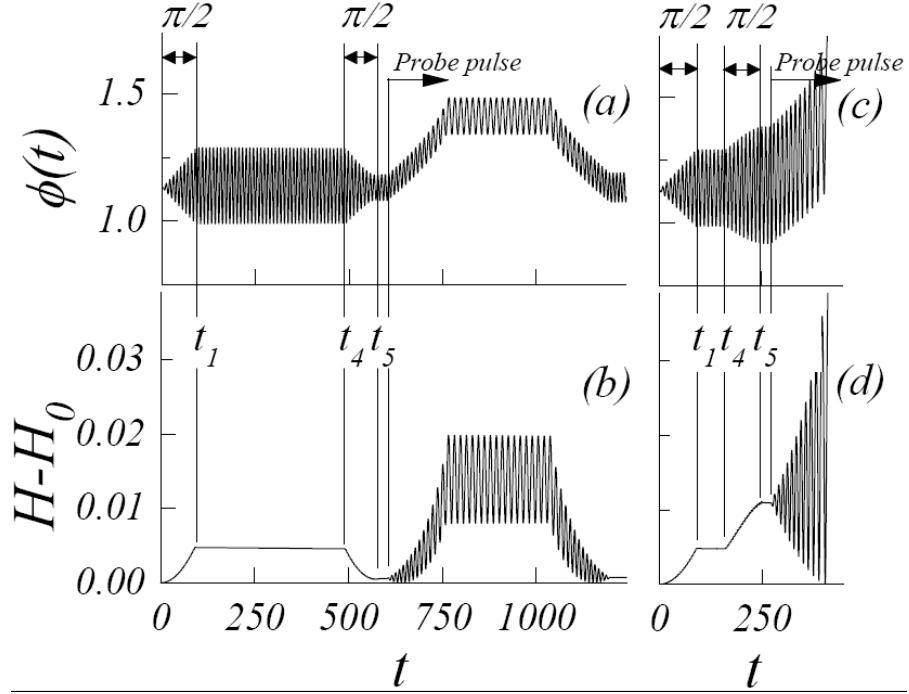


Fig. 5: Direct simulation of the Ramsey-type fringe switching response. Josephson junction response to the sequential application of two $\pi/2$ microwave pulses followed by a probe field. Panels (a,b) show phase-difference and energy for a non-switching sequence in the case of $t_4 - t_1 = 400$. Panels (c,d) indicate a switching event for $t_4 - t_1 = 70$. Parameters were $\alpha = 10^{-4}$, $\eta = 0.904706$, $\varepsilon_s = 2.17 \times 10^{-3}$, $\omega_s = \omega_l = \sqrt[4]{1 - \eta^2} = 0.652714$, $\varepsilon_p = 8.2 \times 10^{-2}$, and $\Theta = 0$.

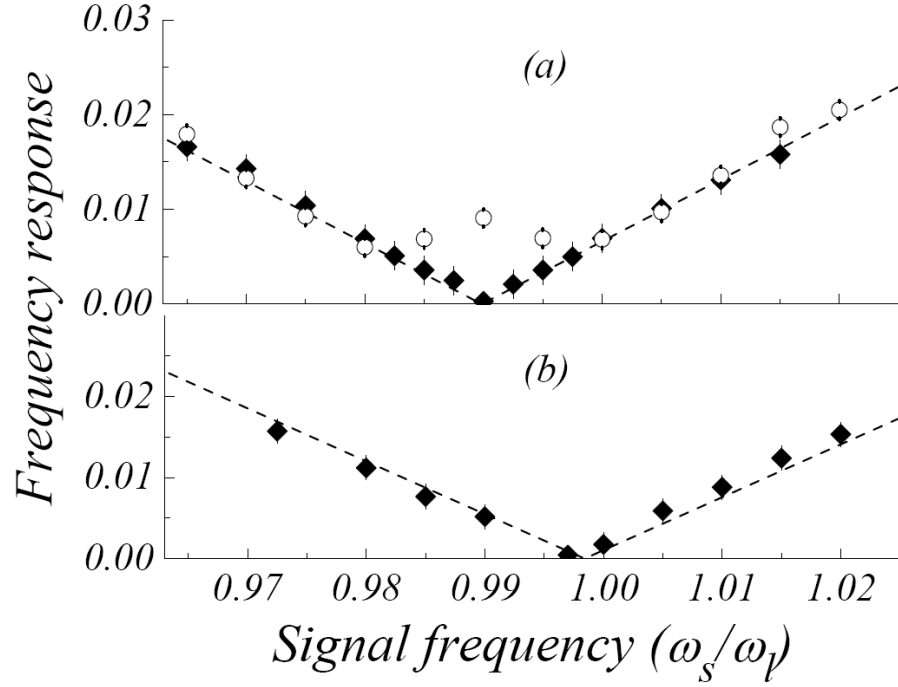


Fig. 6: Frequency response as a function of applied microwave frequency for two different dissipation parameters: (a) $\alpha = 10^{-4}$, and (b) $\alpha = 10^{-3}$. Filled diamonds depict Ramsey-type fringe frequencies, Ω_F , with parameters corresponding to Fig. 4. The open circles in (a) represent spin-echo-type frequencies with parameters as in Fig. 5.

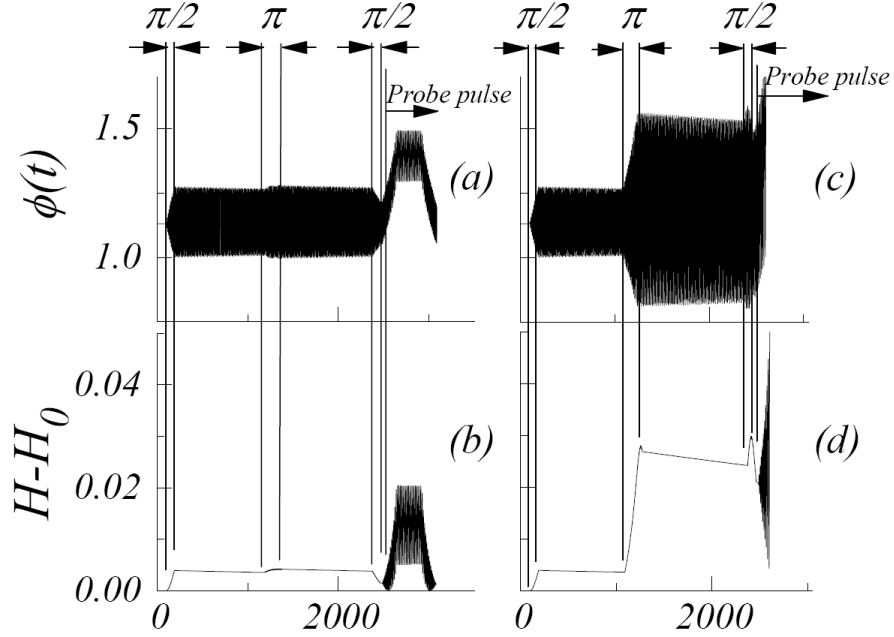


Fig. 7: Direct simulation of the spin-echo-type oscillation switching response. Josephson response to the application of two $\pi/2$ microwave pulses, with an intervening π -pulse, followed by a probe field. The delay between the $\pi/2$ pulses is $t_4 - t_1 = 2182$. The π -pulse offset is for (a,b) (non-switching) $t_2 - t_1 = 1000$. For (c,d) (switching) $t_2 - t_1 = 900$. Parameters were $\alpha = 10^{-4}$, $\eta = 0.904706$, $\varepsilon_s = 2.17 \times 10^{-3}$, $\varepsilon_p = 7.5 \times 10^{-2}$, and $\Theta = 0$.